Mechanism of actin filament branch formation by Arp2/3 complex revealed by a high resolution cryo-EM structure of the branch junction

Steven Z. Chou[1], Moon Chatterjee[1] and Thomas D. Pollard[1,2, 3,*]

[1]Department of Molecular Cellular and Developmental Biology
[2]Department of Molecular Biophysics and Biochemistry
[3]Department of Cell Biology
Yale University, PO Box 208103
New Haven, CT 06520-8103 USA

Supplemental materials

Supplemental Materials and Methods

Actin purification. Chloroform-washed muscle acetone powder was made from flash-frozen chicken skeletal muscle purchased from a local Trader Joe's grocery store. Actin was purified (1) starting with extraction from 4 g of muscle acetone powder using 80 mL of G-buffer (2 mM Tris-HCl, pH 8.0, 0.2 mM ATP, 0.5 mM DTT, 0.1 mM $CaCl_2$, 1 mM NaN_3) at 4°C for 30 min, clarified by centrifugation and polymerized in 50 mM KCl and 2 mM $MgCl_2$ at 4°C for 1 h. Tropomyosin was removed from actin filaments by stirring in 0.8 M KCl at 4°C for 30 min. Actin filaments were pelleted by centrifugation at 140,000× *g* at 4°C for 2 h, dispersed with a Dounce homogenizer and depolymerized by dialysis against 1 L of G-buffer at 4°C. The buffer was changed four times over 3 days. Depolymerized actin was clarified by centrifugation at 135,000× *g* at 4°C for 2 h. The top 2/3 (~10 mL) of the centrifuge tube was applied onto Sephacryl S-300 gel filtration column equilibrated with G-buffer to separate actin oligomers, capping protein and other minor contaminants from the actin monomers (peak tail). Actin concentration was determined using an extinction coefficient of 1 OD_{290} = 38.5 µM. The protein was used in less than two weeks.

Arp2/3 complex. Wild-type Arp2/3 complex was purified from protease-deficient strain of *Schizosaccharomyces pombe* TP150 (2). The cell culture was grown in YE5S at 28°C to OD_{600} ~1.5, when 70 g of YE5S powder per L of liquid culture was added and the cell culture was further grown at 32°C to OD_{600} of ~5. Cells from 8 L of culture were harvested by centrifugation at 6700× *g* for 5 min, and resuspended in 160 mL of U buffer (50 mM HEPES, pH7.5, 100 mM KCl, 3 mM $MgCl_2$, 1 mM EGTA) supplemented with 1× homemade protease inhibitors (1 µM bestatin, 1 µM aprotinin, 1 µM leupeptin, 1 µM pepstatin; dissolved in DMSO) and 1 mM PMSF, frozen in liquid nitrogen and stored at -80°C. Thawed cell pellets were suspended by stirring at 4°C and disrupted by passing 20 times through a cooled Microfluidizer (model M-110EH, Microfluidics, Westwood, MA) at 25,000 psi. Large cell debris was removed by centrifugation at 47,000× *g* at 4°C for 20 min, followed by centrifugation at 4°C and 214,000× *g* for 1 h. Proteins were precipitated by adding ammonium sulfate gradually to 30% saturation, pelleted by centrifugation at 167,000× *g* at 4°C for 30 min, resuspended in 50 mL of PKME buffer (25 mM PIPES, pH 6.5, 50 mM KCl, 3 mM $MgCl_2$, 1 mM EGTA, 0.1 mM ATP, 1 mM DTT) supplemented with 1× homemade protease inhibitors, and dialyzed against two changes of 2L of the same buffer in a 50 kDa MWCO tubing overnight. The dialyzed sample was clarified

by centrifugation at 150,000× *g* at 4°C for 1 h before being applied onto a Glutathione Sepharose affinity column (bed volume: ~2.5 mL) prebound with 16 mg of GST-SpWsp1p-VCA (residues 497-574) and equilibrated with 20 mL of PKME (25 mM PIPES, pH 6.5, 50 mM KCl, 3 mM $MgCl_2$, 1 mM EGTA, 0.1 mM ATP, 1 mM DTT) buffer. After washing 5 times with 5 mL of PKME and 5 times with 10 mL of PKME-150 (25 mM PIPES, pH 6.5, 150 mM KCl, 3 mM $MgCl_2$, 1 mM EGTA, 0.1 mM ATP, 1mM DTT). The bound Arp2/3 complex was eluted from the affinity column with QB buffer (10 mM PIPES, pH 6.8, 1000 mM NaCl, 1 mM $MgCl_2$, 1 mM EGTA, 0.1 mM ATP, 1 mM DTT). Fractions containing Arp2/3 complex were pooled and dialyzed against 2 L of QD buffer (10 mM PIPES, pH 6.8, 25 mM NaCl, 0.25 mM $MgCl_2$, 0.25 mM EGTA, 0.1 mM ATP, 1 mM DTT) for 1 h twice. The sample was filtered through a 0.22-µm PVDF syringe filter before being applied to a MonoQ ion exchange column 5/50 GL (GE Healthcare) equilibrated with QA buffer (10 mM PIPES, pH 6.8, 50 mM NaCl, 1 mM $MgCl_2$, 1 mM EGTA, 0.1 mM ATP, 1 mM DTT), and then eluted with a gradient 0% to 30% QB buffer over 40 column volumes. The fractions containing the complex were combined (< 5 mL in total) and gel filtered through a Superdex 200 16/600 column using QB buffer. The Arp2/3 complex concentration was determined using an extinction coefficient of 1 OD_{290} = 7.19 µM. The complex was supplemented with 5% glycerol, flash-frozen in liquid nitrogen and stored at -80°C.

GCN4-VCA purification. A DNA fragment encoding a PreScission protease cleavage site, *Saccharomyces cerevisiae* GCN4 leucine-zipper (residues 249-281) and bovine N-WASP residues 401-505 (the VCA motif) was synthesized (IDT, Inc., Coralville, Iowa) and inserted to pQE-BhT vector digested with BamHI and HindIII. The resulting plasmid pQE-BhT-GCN4-N-WASP-VCA was confirmed by sequencing and transformed into Rosetta 2 (DE3) *E. coli* competent cells. Cells were shaken in 8 L of LB medium at 37°C to an OD_{600} of 0.8. Protein expression was induced by adding IPTG to 0.2 mM and shaking at 22°C overnight. The fusion protein was purified using a gravity-driven Ni-NTA column (bed volume: 5 mL; Qiagen), eluted with NE buffer (50 mM Tris-HCl, pH 8.0, 500 mM NaCl; 300 mM imidazole). The eluted protein was dialyzed against 1 L of PD buffer (10 mM Tris-HCl, pH 8.0, 100 mM NaCl, 1 mM DTT) for 1 h at 4°C to remove imidazole before being digested with homemade PreScission protease at a 100:1 ratio of [protein]/[protease] for 16 h. The digested protein was dialyzed at 4°C against three changes of 1 L of NW buffer (50 mM Tris-HCl, pH 8.0, 500 mM NaCl) over 9 h before being applied onto the second Ni-NTA column to remove the fusion tag and protease.

The protein in flow-through was concentrated to ~3.0 ml using a Millipore centrifugal filter unit with a MWCO of 10 kDa and then further purified by gel filtration on a Superdex 75 16/600 column equilibrated with KHT buffer (100 mM KCl, 10 mM HEPES, pH 7.0, 0.4 mM TCEP). The concentration was determined by absorbance at 280 nm using an extinction coefficient of 1 OD_{280} = 143.1 μM calculated using the online ProtPram tool. Aliquots of purified protein were frozen in liquid nitrogen and stored at -80°C.

Capping protein purification. The two subunits of mouse CapZ α1/β heterodimer were co-expressed in Rossetta 2 (DE3) cells using the pRSFDuet1-His6-CapZα1:β plasmid (Addgene plasmid #: 89950) at 22°C overnight. The protein was purified from the soluble fraction of lysed bacteria by Ni-NTA affinity chromatography, concentrated using a Millipore centrifugal filter unit with a MWCO of 30 kDa and then gel filtered on a Superdex 200 16/600 column equilibrated with KH buffer (100 mM KCl, 10 mM HEPES, pH 7.0). Its concentration was determined using an extinction coefficient of 1 OD_{280} = 70.0 μM. Fractions from the heterodimer peak were aliquoted, frozen in liquid nitrogen and stored at -80°C.

Assembly of specimens with short branches. The Ca^{2+} bound to actin monomers was exchanged for Mg^{2+} by incubating 50 μL of 22.5 μM Ca-ATP-actin monomers with 0.1 volumes of 10× ME buffer (0.5 mM $MgCl_2$, 2 mM EGTA, pH 7.5) at room temperature for 10 min. Actin monomers were polymerized into filaments by sequentially mixing 15 μL of 3.2 μM capping protein in 100 mM KCl, 10 mM HEPES, pH 7.0, 20 μL of 1× KMEH buffer (100 mM KCl, 1 mM $MgCl_2$, 1 mM EGTA, 10 mM HEPES, pH 7.0, 1 mM DTT), and 35 μL of 20 μM Mg-ATP-actin monomers and incubating at room temperature for 1 h. Separately, 1.0 μL of 25 μM Arp2/3 complex in QB buffer was pre-activated by mixing with 1.15 μL of 50 μM GCN4-VCA in KHT buffer and 1.0 μL of 10 mM ATP (pH 7.0 in H_2O) and incubating at 4°C for 1 h before mixing with 70 μL of capped actin filaments from the previous step and incubating at room temperature for 5 min. Capped daughter filaments were grown in five cycles by adding sequentially to Arp2/3 complex with capped mother filaments 1.0 μL of 0.1 mM ATP, 1.0 μL of 3.2 μM capping protein and 1.0 μL of 20.3 μM Mg-ATP-actin monomers. After each cycle samples were incubated at room temperature for 5 min. The final sample of 88 μL contained in addition to the capped mother filaments 0.28 μM Arp2/3 complex, 1.15 μM actin and 0.18 μM capping protein. The sample was used directly for vitrification in the next step without dilution. The density of

branch junctions in electron micrographs of negatively stained specimens did not decrease overnight 4°C, so the branches were stable for hours.

Sample freezing and image acquisition. Holy carbon Quantifoil 1.2/1.3 300-mesh Au grids were used directly without glow-discharging. To freeze the sample, 3.0 µL of branched actin filaments were applied onto the carbon side of the grid in Mark IV Vitrobot at 4°C and ~100% humidity. After incubating on the grid for 50 s, extra solution was blotted off using standard Vitrobot filter paper (Ø55/20 mm, Grade 595, Ted Pella) for 4.0 s at 0 blot force. The grids dwelled in the Vitrobot humidity chamber for 0.5 s before plunging into liquid ethane cooled to about -180°C. The vitrified grids were screened in a Glacios electron microscope operated at 200 kV and equipped with a Gatan K3 summit camera (FEI company, Hillsboro, OR). Electron micrographs for image reconstruction were collected from two grids in a Titan Krios microscope equipped with a XFEG at 300 kV, a nanoprobe, and a Gatan image filter (slit width: 20 eV). Movies were recorded at a series of defocus values between -2.5 µm and -1.2 µm on a K3 Summit camera in super-resolution mode, using the beam image shift strategy (9 movies/stage movement; 1 movie per hole) implemented in SerialEM. Each movie had 41 frames and each frame time was 0.08 s. The dose rate at camera level was 28.4 counts/pixel/s, and physical pixel size was 1.364 Å.

EM image processing. The dataset of images was processed mostly using Relion 4.0 (3), including the steps from motion correction and CTF estimation to map post-processing. Standalone Topaz (4) was used for initial AI-based particle picking. Topaz reliably identified branches with the daughter filament lying approximately in the x-y plane of the grid but missed virtually all branches oriented parallel or almost parallel to the z-axis. Three dimensional reconstructions with this incomplete data set were highly distorted, due to the absence of particles with branches along the z-axis. We found that visual inspection and hand picking assisted by a program (https://github.com/stevenzchou/Fesp) to catalog the coordinates of the branches was the only reliable way to include the branches oriented along the z-axis for image processing, which depends on having a random sample of orientations around at least one great circle. We used Relion to make a 3D reconstruction from a sample of 79,467 particles selected from 131,393 hand-picked branches. The resolution of the map was better than 3.5 Å (Table 1), sufficient for model building. The map sphericity was calculated with 3DFSC. The correlation between the map and the model was calculated with PHENIX.

Model building and refinement, and structural analysis and visualization. Our map allowed us to build models for most residues unambiguously in Coot (5). We also used a model of the Arp2/3 complex determined by cryo-EM (PDB: 6W18) and model of the individual subunits of Arp2/3 complex generated by AlphaFold (6) as references for cross-validation. Our model of Arp2/3 complex is more complete than previous models, because many regions of Arp2/3 complex in the branch junction are more rigid than in isolated Arp2/3 complex used for previous structural studies. We refined the modeled structure using PHENIX (7) in real space. Interdomain rotation angles were calculated with PyMOL. Rise (subunit translation) and twist (subunit translation), RMSDs, and buried surface areas were calculated using Chimera (8). Figures were generated using ChimeraX (9).

Table S1. The rise and twist between actin subunits and/or Arp subunits.

Subunits	Rise (Å)	Twist (°)
M1 and M2	27.73	-166.50
M2 and M3	27.84	-167.21
M3 and M4	27.77	-167.37
M4 and M5	27.80	-166.29
M5 and M6	27.77	-167.13
Arp3 and Arp2	28.19	-166.27
Arp2 and D1	27.83	-168.64
D1 and D2	27.97	-166.87
ADP-actin filaments	27.60	-166.66

The rise and twist between Arp2 and actin D1, and between actin D1 and actin D2 are almost identical to those in Dip1-activated Arp2/3 complex except for between Arp3 and Arp2 (10).

Table S2. Buried solvent accessible surface areas (Å^2) between subunits of Arp2/3 complex and subunits (M1-M6) in the mother filament.

Active Arp2/3 complex in branch junction

	M1	M2	M3	M4	M5	M6	Buried surface
Arp3	0	0	158	348	0	0	506 Å^2
Arp2	0	0	0	0	0	0	0 Å^2
ARPC1	0	104	0	491	0	0	595 Å^2
ARPC2	595	300	39	358	0	0	1292 Å^2
ARPC3	0	0	0	0	0	176	176 Å^2
ARPC4	0	753	0	0	0	0	753 Å^2
ARPC5	0	59	0	0	0	0	59 Å^2

Red text = reported by Fäßler et al. (11). Shading = reported by Rouiller et al.(12).
Total buried surface: 3381 Å^2 by sum of individual contacts
Total buried surface: 3337 Å^2 by whole Arp2/3 complex

Inactive Arp2/3 complex docked onto an actin filament by ARPC2 and ARPC4

	M1	M2	M3	M4	M5	M6	Buried surface
Arp3	0	0	0	198	0	0	198 Å^2
Arp2	0	0	0	0	0	0	0 Å^2
ARPC1	0	0	0	0	0	0	0 Å^2
ARPC2	758	244	24	0	0	0	1026 Å^2
ARPC3	0	0	0	0	0	0	0 Å^2
ARPC4	0	970	0	0	0	0	970 Å^2
ARPC5	0	12	0	0	0	0	12 Å^2

Total buried surface: 2206 Å^2 by sum of individual contacts

Table S3. Buried solvent accessible surface areas (Å^2) between subunits of Arp2/3 complex.

Inactive Arp2/3 complex

	Arp3	Arp2	ARPC1	ARPC2	ARPC3	ARPC4	ARPC5
Arp3							
Arp2	451						
ARPC1	0	139					
ARPC2	1511	0	11				
ARPC3	606	0	0	0			
ARPC4	213	833	1137	2309	0		
ARPC5	0	0	561	0	0	899	

Active Arp2/3 complex in branch junction

	Arp3	Arp2	ARPC1	ARPC2	ARPC3	ARPC4	ARPC5
Arp3							
Arp2	671						
ARPC1	0	296					
ARPC2	1502	165	229				
ARPC3	898	639	0	0			
ARPC4	280	884	1161	2133	0		
ARPC5	0	612	541	0	0	1006	

Difference = active – inactive

	Arp3	Arp2	ARPC1	ARPC2	ARPC3	ARPC4	ARPC5	Sum
Arp3								
Arp2	220							+220
ARPC1	0	157						+157
ARPC2	-9	165	218					+374
ARPC3	292	639	0	0				+931
ARPC4	67	51	24	-176	0			-34
ARPC5	0	612	-20	0	0	107		+699

Large differences are highlighted in red. Total change is +2347 Å^2.

Table S4. Regions with backbone changes.

ROI	Actin monomer vs. filament	Arp2: inactive Arp2/3 complex vs. branch	Arp3: inactive Arp2/3 complex vs. branch
N-terminus	88; 1-9	**150; 1-7**	**150; x-9**
ß1-ß2 loop	<37; 13-16	<39; 13-16	**176; 10-19**
ß4-ß5 loop (D-loop)	**Disordered → ordered; 39-50**	**Disordered → ordered; 39-50**	**Disordered; 38-68**
ß5-H1 loop	<33; 50-56	61; 50-56	100; 68-77
H1-ß6 loop	<14; 61-65	<30; 61-65	**154; 86-92**
H2-ß7 loop	<40; 94-103	**180; 97-109**	61; 114-120
ß7-H3 loop	<44; 108-112	16; 108-111	142; 149-157
H4 hinge helix	<35; 137-144	<20;137-145	<24; 160-167
H4-ß9 loop	<35; 145-150	80; 145-151	**160; 169-180**
ß10-ß11 loop (W-loop)	113; 160-170;	<48; 160-170	**108; 196-203**
ß11-H5 loop	<49; 179-182	78; 179-182	74; 210-213
H5-H6 loop	75; 195-203	**145; 197-212**	**Disordered → ordered; 224-235**
H6-H7 loop	<24; 216-223	81; 216-223	**153: 239-250**
H7-ß12 loop	102; 231-239	<25; 231-230	**Disordered → ordered; 258-267**
ß12- ß13 loop	<20; 241-247	<50; 242-246	**Disordered → ordered; 271-280**
H8-H9 loop; H plug	67; 262-270:	**142:266-275**	80 ;294-305
ß14-H11 loop	<24; 300-309	71; 300-309	88; 330-345
H11-ß15 strand loop	73; 321-328	70; 321-324	**174: 364-375**
H13-H14 loop	<23; 355-359	**178; 367-373**	<54’ 401-406
H14-C-terminus	Disordered → helix; 365-375	Disordered; 386-390	110; 410-427

Entries are absolute values of the maximum dihedral angle differences; residues involved.

Color code: Difference < 50°; Difference = 50-150; **Difference > 150**

Dihedral phi and psi angles were taken from pdb files 2A42 for actin monomer, 6DJN for actin filament, 6W18 for inactive Arp2/3 complex and 8E9B for active Arp2/3 complex.

Table S5. Flattening actin and Arps during polymerization. Inactive is actin monomer or inactive Arp2/3 complex. Active is actin polymer or Arp2/3 complex in branch junction. Dip1 is Arp2/3 complex bound to Dip1 and a daughter filament. Widths of the nucleotide-binding clefts were measured from distances between two residues: Actin, S14 Cα–G158 Cα; Arp2, T12 Cα–G158 Cα; Arp3, T14 Cα–G189 Cα.

	Nucleotide-binding cleft (Å)				Dihedral angle SD1/2 vs. SD3/4 (degrees)			
	Inactive	Active	Dip1	Δ inactive vs. Active; Dip1	Inactive	Active	Dip1	Δ inactive vs. Active; Dip1
Actin	5.4	5.2		-0.3	-14.7	-0.7		+14.0 (DNase) +18.7 (TMR)
Arp2	7.7	5.1	5.9	-2.6; -1.8	-10.1	+1.2	-1.5	+11.3; +8.5
Arp3	9.7	5.1	5.8	-4.6; -3.9	-18.2	-4.5	-10.9	+13.7; +7.3

Table S6. Comparison of branch junction structures

Feature	Ding et al.	Chou et al.
Source of Arp2/3 complex	Bovine	*S. pombe*
Source of actin	Chicken	Chicken
NPFs	N-WASP VCA, Spin 90, cortactin	GCN4-N-WASP VCA
Other constituents	Phalloidin, capping protein	Capping protein
Resolution	3.9 Å	3.4 Å
Nucleotide bound to actin	ADP	ADP
Nucleotide bound to Arps	Arp2, Arp3 ADP	Arp2 ATP, Arp3 ADP
Arp dihedral angles in branch	Arp2 -3.7°, Arp3 -5.8°	Arp2 +1.2°, Arp3 -4.5°
Change of internal buried surface area during branch formation	**391 Å^2**	**2347 Å^2**
Arp2/3 complex surface area buried on mother filament	Inactive 1872 Å^2 Active, 3727 Å^2	Inactive 2,206 Å^2 Active 3381 Å^2
Mother filament subunits contacting Arp2/3 complex	M1, M2, M3, M4, M6 not distorted	M1, M2, M3, M4, M6 not distorted
Arp2/3 complex subunits contacting mother filament with buried surface area (Å^2)	Arp2 (0), Arp3 (1156), ARPC1 (480), ARPC2 (997), ARPC3 (189), ARPC4 (730), ARPC5 (175)	Arp2 (0), Arp3 (506), ARPC1 (595), ARPC2 (1292), ARPC3 (176), ARPC4 (753), ARPC5 (59)
Arp2/3 complex surface area (Å^2) buried on daughter filament	Inactive 0 Active 2896 Å^2	Inactive 0 Active 2986 Å^2
Arp3 C-terminus	Moves from B-end groove and interacts with actin and Arp2	Moves from B-end groove and interacts with actin and Arp2
ARPC2/4 helix rotation	-20°	-15° to -25° depending on residues tested
Rotation & translation of Arp2 block	Rotates 19°, <Dip1 complex, moves CM Arps by ~19Å	Depends on residues tested
Differences between the two branch structures	Arp3 D-loop ordered (22 residues) ARPC1 Both insert helix loops ordered ARPC2 C-terminus disordered	Arp2 C-terminus better ordered Arp3 36 D-loop residues mostly disordered ARPC1 N-terminal insert helix loop disordered ARPC2 C-terminus ordered, contacts actin M4 & Arp2; extra residues 134-151 interact with actin M1

Orange text indicates a major difference.

Table S7. Buried solvent accessible surface areas (Å^2) between subunits of Arp2/3 complex.

Inactive *S. pombe* Arp2/3 complex vs. bovine Arp2/3 complex. Bold, large differences.

	Arp3	Arp2	ARPC1	ARPC2	ARPC3	ARPC4	ARPC5	Total
Arp3								
Arp2	**451/871**							**451/871**
ARPC1	0/0	139/227						139/227
ARPC2	1511/1697	0/0	11/38					1522/1735
ARPC3	**606/925**	0/0	0/0	0/0				**606/925**
ARPC4	**213/562**	833/793	1137/1167	2309/2199	0/0			4492/4721
ARPC5	0/0	**0/658**	561/706	0/0	0/0	899/958		1460/2322
Total	2781/4055	**972/1678**	1709/1911	2309/2199	0/0	899/958		**8670/10801**

Active Arp2/3 complex in branch junction

	Arp3	Arp2	ARPC1	ARPC2	ARPC3	ARPC4	ARPC5	Total
Arp3								
Arp2	671/689							671/689
ARPC1	0/0	296/260						296/260
ARPC2	1502/1673	165/0	229/212					1896/1885
ARPC3	898/972	639/719	0/0	0/0				1537/1691
ARPC4	280/**498**	884/780	1161/1080	2133/2212	0/0			4458/4570
ARPC5	0/0	612/505	541/609	0/0	0/0	1006/958		2159/2072
Total	3351/3832	2596/2264	1931/1901	2133/2212	0/0	1006/958		11017/11167

Difference = active – inactive

	Arp3	Arp2	ARPC1	ARPC2	ARPC3	ARPC4	ARPC5	Total
Arp3								
Arp2	**220/-182**							+220/-182
ARPC1	0/0	**157/33**						**+157/+33**
ARPC2	-9/-24	**165/0**	218/174					**+374/+150**
ARPC3	**292/47**	639/719	0/0	0/0				+931/+766
ARPC4	67/-64	51/-13	**24/-87**	**-176/13**	0/0			-34/-151
ARPC5	0/0	**612/-153**	-20/-97	0/0	0/0	107/25		**+699/-225**
Total	**570/-223**	**1624/586**	**222/-10**	**-176/13**	0/0	107/25		**+2347/+391**

Total change is +2347 Å^2 for *S. pombe* and +391 Å^2 for bovine.

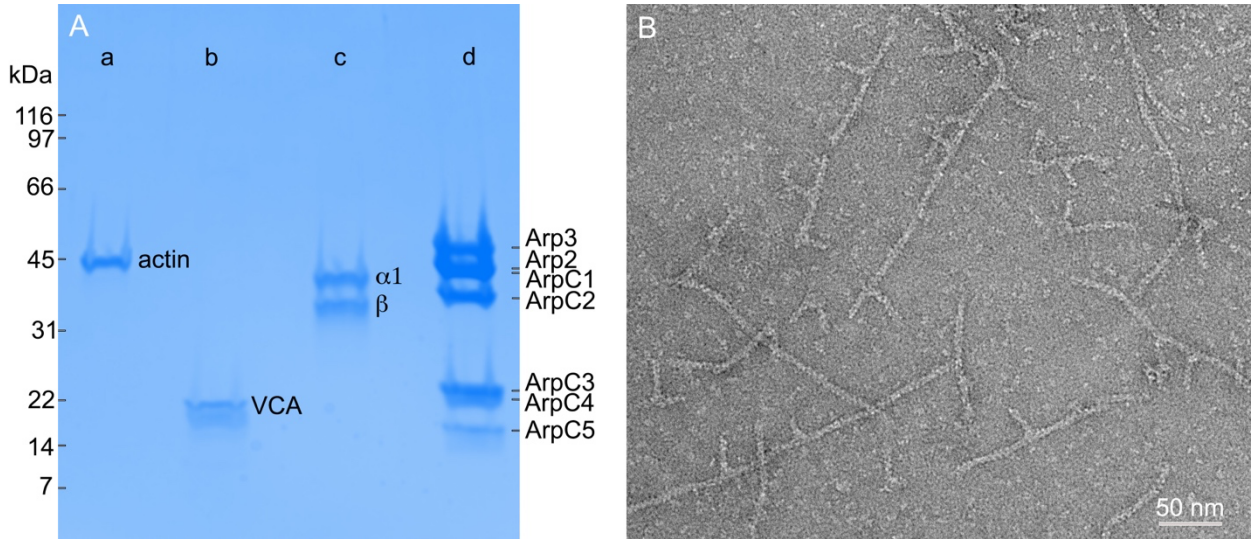

Fig. S1. Quality assessment of individual protein components and assembly of the components into actin branch junctions. (*A*) SDS-PAGE of the purified proteins used to assemble branch junctions. Lane a: actin monomers (MW: ~42 kDa) isolated from chicken skeletal muscle (UniProt ID: P68139). Lane b: the VCA motif (residues 401-505) of bovine N-WASP (UniProt ID: Q95107) fused to the C-terminus of the leucine zipper motif (residues 249-281) of budding yeast GCN4 (UniProt ID: P03069) (MW of the fusion protein: 15.9 kDa). Lane c: the His_6-tagged α1 (MW: 33.9 kDa) and tag-free β (MW: 30.6 kDa) subunits of the heterodimeric mouse barbed end capping protein. Lane d: seven subunits (Arp3: 47.3 kDa; Arp2: 44.2 kDa; ARPC1: 41.6 kDa; ARPC2: 37.0 kDa; ARPC3: 19.8 kDa; ARPC4: 19.6 kDa; ARPC5: 16.9kDa) of fission yeast *S. pombe* Arp2/3 complex. (*B*) Electron micrograph of negatively stained branched actin filaments. Most of the mother filaments are between 100 nm and 400 nm long, and most daughter filaments (composed of Arp2/3 complex, actin subunits and capping protein) are between 30 nm (~7 actin subunits) and 60 nm (~18 actin subunits). A sample of 26 branches had an average length of 15.4 (SD 2.0) subunits.

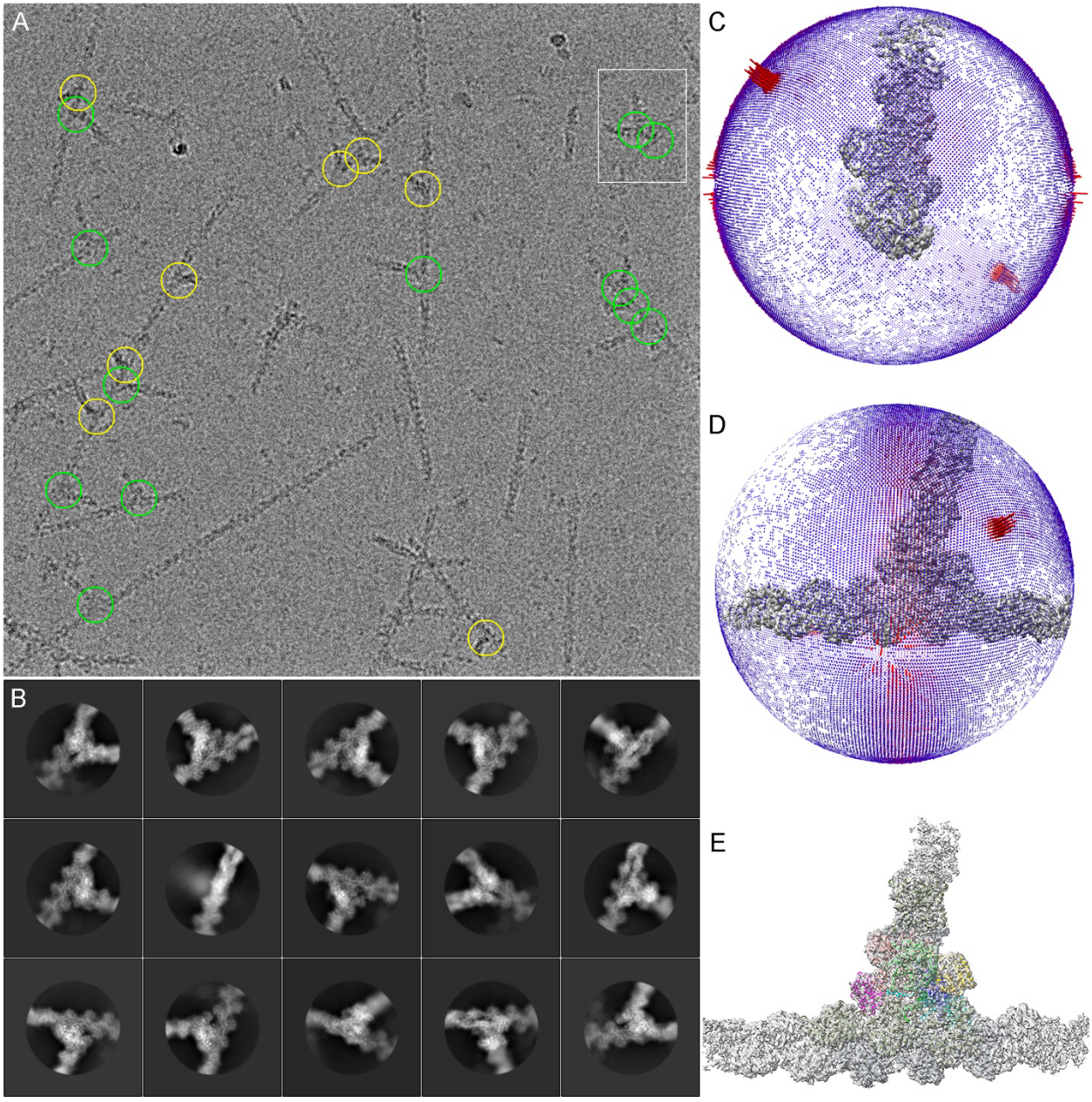

Fig. S2. Strategy for solving the missing angle problem in EM map reconstruction. *(A)* A representative electron micrograph showing the decoration of long mother filaments with Arp2/3 complex and short daughter filaments arranged around the mother filament at different angles. Autopicking using neural networks can identify branches with the daughter filaments oriented roughly perpendicular to the electron beam (highlighted in green circles). The density of these daughter filaments is similar to that of the mother filaments. The densities of branches oriented

roughly parallel to the electron beam (yellow circles) are higher than mother filaments. Manual picking is required to identify these vertical branches. A white box in the upper right corner highlights two branches – the daughter filament of one branch is the mother filament for the other branch. The ice thickness was estimated to be between 70 and 130 nm to reduce the preferred orientation of the branches. *(B)* Representative 2D class averages of the branch junction. *(C and D)* The angular distributions of particles used for the final reconstruction showed a preferred orientation but no missing angles for the great circle around the mother filament. The barbed end of the mother filament points at the reader in (*C*) and to the right in (*D*). The number of particles in each sampled orientation is indicated by both the height and color of the bar; blue: low; red: high. *(E)* Reconstructed 3D map fitted with a model showing no distortion.

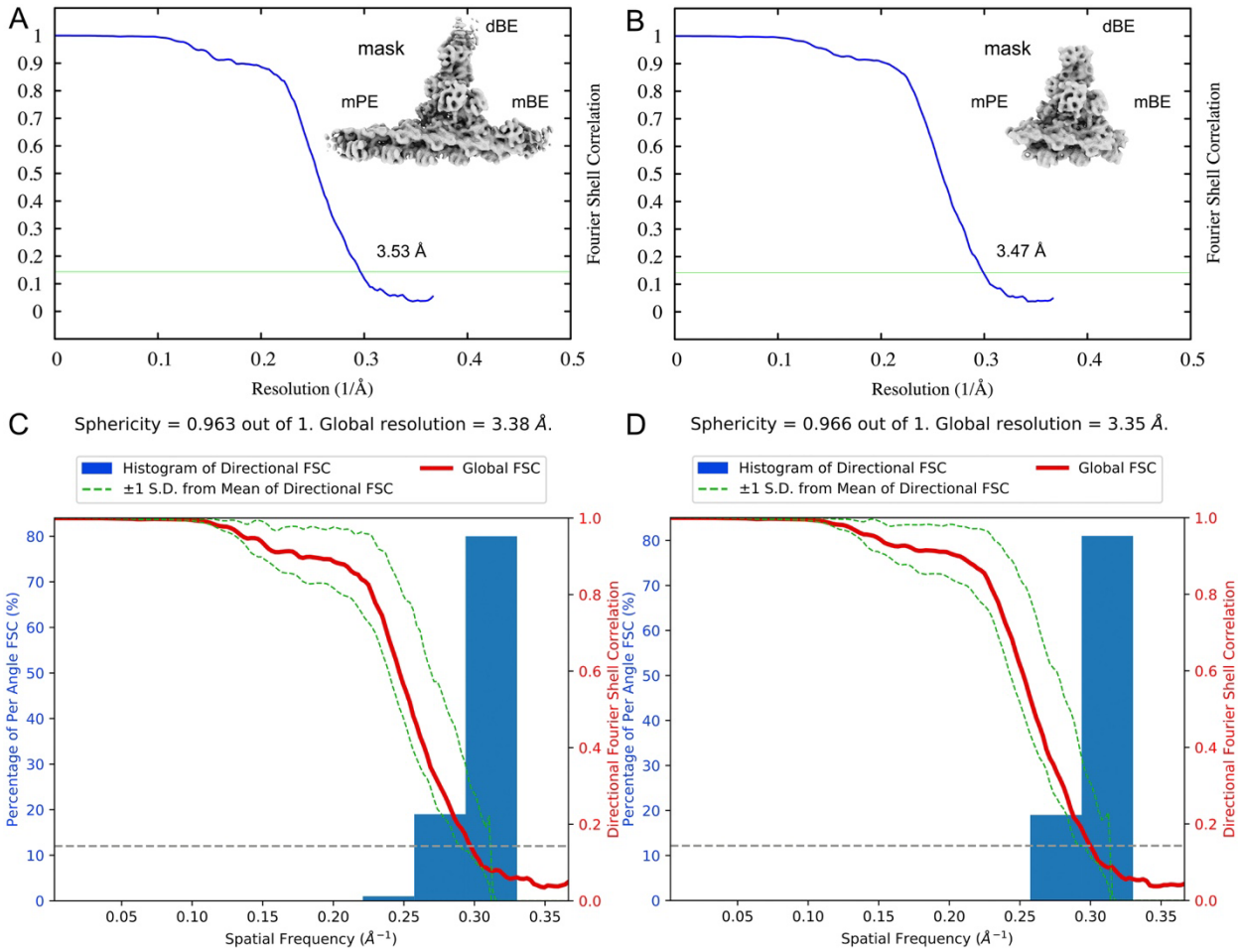

Fig. S3. Resolution estimation. *(A, C)* Calculated for the full reconstruction. *(B, D)* Calculated for the Arp2/3 complex, five mother filament subunits and 2 daughter filament subunits. *(A, B)* Global resolution of actin filament branch map estimated using Fourier shell correlation (FSC, blue curve) with 0.143 criterion (green horizontal line). *(C, D)* Global resolution and map sphericity calculated with 3DFSC. The insets show the masks used for these calculations.

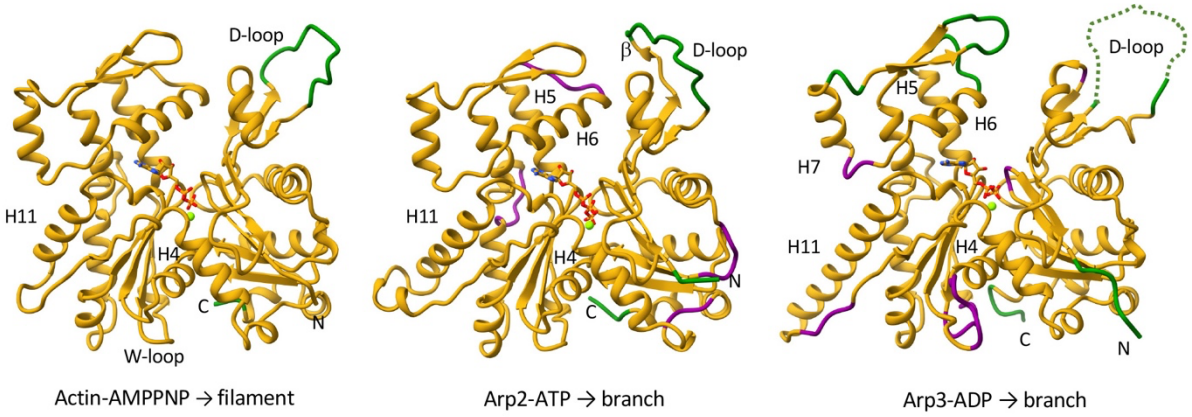

Fig. S4. Flattening Arp2 and Arp3 during branch formation involves many more changes in backbone dihedral angles than flattening actin during polymerization. See Table S4 for details. Ribbon diagrams with stick figures of bound nucleotides show the locations of major changes in backbone dihedral angles contributing to conformational changes of (*A*) actin-AMPPNP during polymerization and of (*B*) Arp2-ATP and (*C*) Arp3-ADP during branch formation. Backbone segments are color coded: purple for segments with dihedral angle changes >150°; green for disordered segments that become ordered during actin polymerization or branch formation; and green dotted for a disordered segment in the branch junction. The β label on Arp2 indicates the segment that forms a β-sheet with ARPC3.

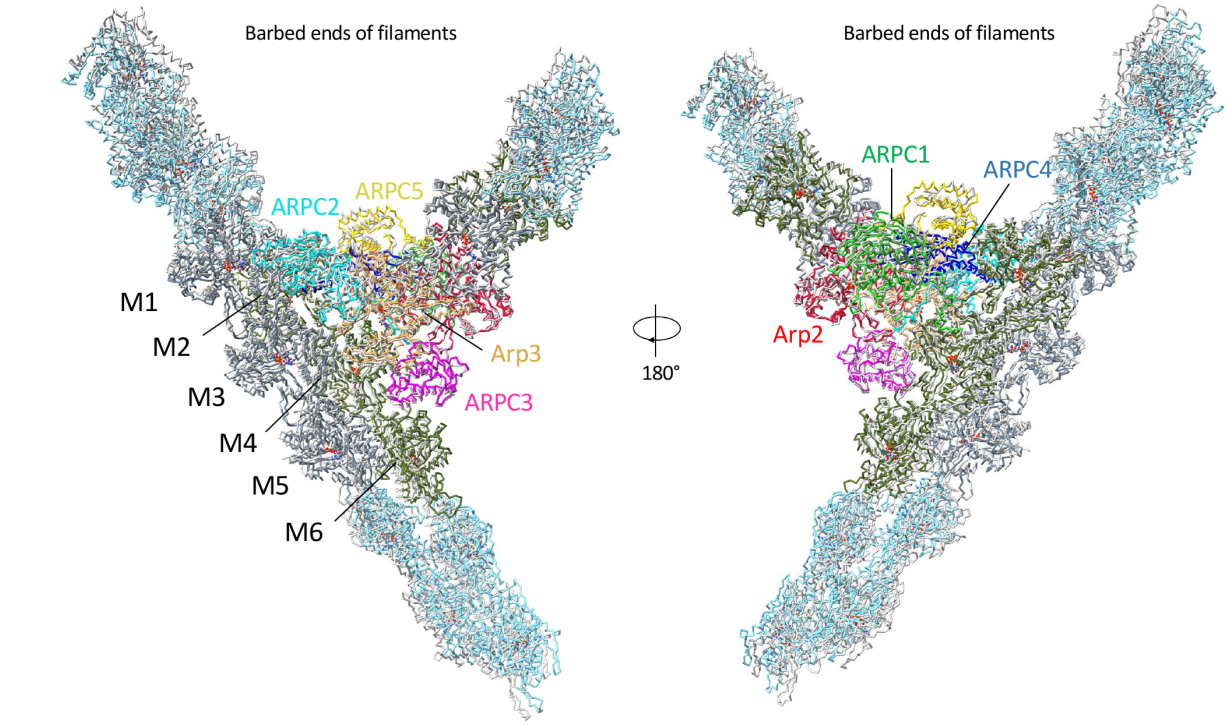

Comparison of subunit structures: Ding grey with plum highlights; Chou colors with purple highlights.

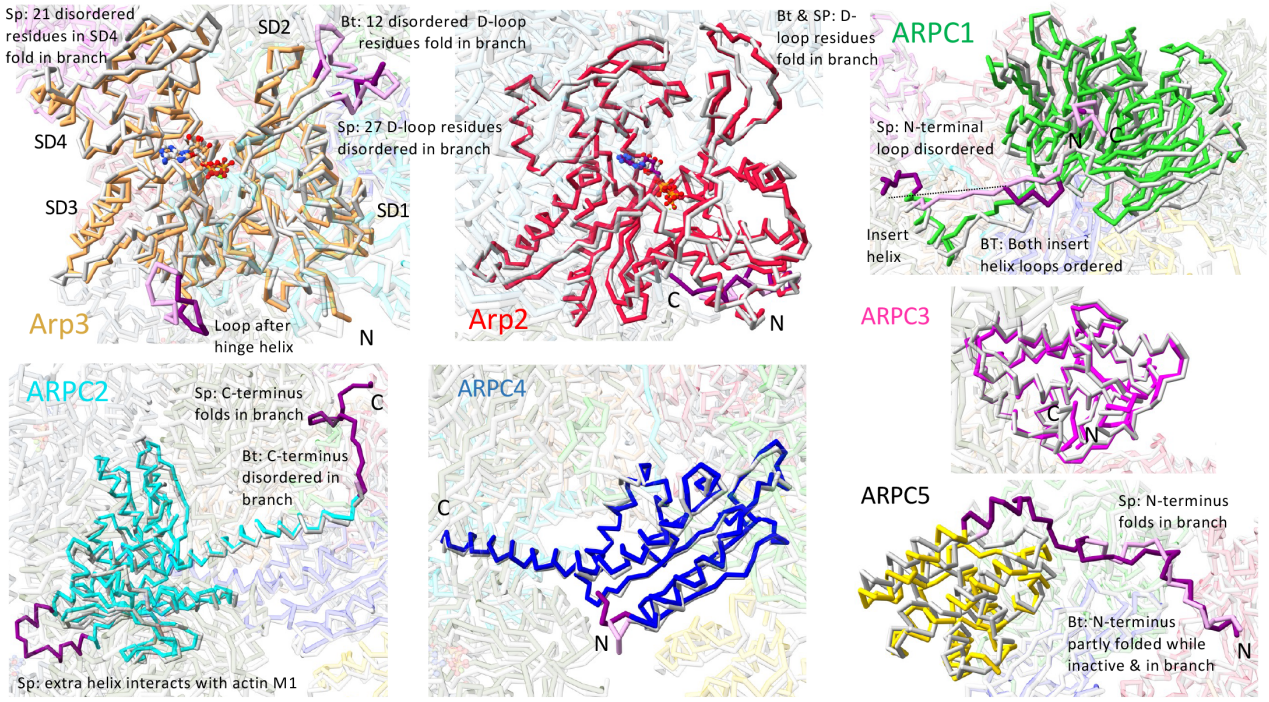

Fig. S5. Branch junction structures formed by bovine and *S. pombe* Arp2/3 complex

Superimposed backbone traces of the *S. pombe* branch junction and the bovine (13) branch junction. The *S. pombe* subunits are the traditional colors with actins outside the core light blue; the bovine subunits are grey. Major differences (*S. pombe*, purple; bovine, plum) in each subunit:

Arp3: The bovine D-loop (K38-D59) of 22 residues is fully ordered; the *S. pombe* D-loop of 36 residues (R38-D73) is mostly disordered (residues A40-S66). The loop after the hinge helix differs slightly.

Arp2: C-termini differ in conformation. The bovine C-terminus is missing 6 residues; *S. pombe* only one missing residue. The bound nucleotide is ATP in *S. pombe* Arp2 and ADP in bovine Arp2, likely because specimen preparation was longer.

ARPC1: The bovine insert helix consists of 11 residues (A298-K308), while the *S. pombe* insert helix has 15 residues (S316-K330). Both contact actin subunits M2 and M4. The bovine connecting loops (V287-T297; A309-K326) are ordered, but the longer *S. pombe* N-terminal connecting loop (A292-V315) is partially disordered (T297-E312). Sequence alignment indicates that the C-terminus of bovine ARPC1 is 13 residues longer than *S. pombe* ARPC1, and the first 5 residues are ordered in the bovine structure.

ARPC2: The map has no density for the C-terminus of bovine ARPC2 (A284-R300, 17 residues), while the C-terminus of *S. pombe* ARPC2 (V301-A317, 17 residues) is ordered and contacts Arp2 and actin M4. *S. pombe* has an 18-residue insertion (residues A134-A151), which forms a bent helix and contacts actin M1.

ARPC3: The C-terminus of bovine ARPC3 is 5 residues longer than *S. pombe* ARPC3.

ARPC4: Structures are nearly identical except slightly different N-terminal conformations.

ARPC5: The N-terminus (residues M1-G36) of bovine ARPC5 has two disordered regions (residues M1-S8 and E27-Q34). The N-terminus of *S. pombe* ARPC5 (residues M1-S37) only has one missing residue from the map, M1. *S. pombe* T2 is in the position of bovine R10.

Supplemental Movie 1. Proposed pathway of branch formation. Step 1, inactive Arp2/3 complex is docked to the side of a mother filament using the interactions of the two globular domains of ARPC2 and the outer domain of Arp3 in the branch junction. Inactive Arp2/3 complex binds weakly and transiently (not shown). Step 2: Morphing from the structure of inactive Arp2/3 complex to its structure in the branch junctions shows the rotation of the two blocks of structure bringing Arp2 and Arp3 together in a short-pitch conformation and flattening both Arps. Step 3, the flattened Arps, aligned in the short-pitch conformation, nucleate the daughter filament.

References

1. MacLean-Fletcher S & Pollard TD (1980) Identification of a factor in conventional muscle actin preparations which inhibits actin filament self-association. *Biochem. Biophys. Res. Commun.* 96(1):18-27.
2. Ti S-C, Jurgenson C, Nolen BJ, & Pollard TD (2011) Structural and biochemical characterization of two binding sites for nucleation promoting factor WASp-VCA on Arp2/3 complex. *Proc. Natl. Acad. Sci. USA* 108:E463-471.
3. Kimanius D, Dong L, Sharov G, Nakane T, & Scheres SHW (2021) New tools for automated cryo-EM single-particle analysis in RELION-4.0. *Biochem J.* 478:4169-4185.
4. Bepler T*, et al.* (2019) Positive-unlabeled convolutional neural networks for particle picking in cryo-electron micrographs. *Nat Methods* 16:1153-1160.
5. Emsley P, Lohkamp B, Scott WG, & Cowtan K (2010) Features and development of Coot. *Acta Crystallogr. D Biol. Crystallogr.* 66(Pt 4):486-501.
6. Jumper J*, et al.* (2021) Highly accurate protein structure prediction with AlphaFold. *Nature* 596:583-589.
7. Adams PD*, et al.* (2010) PHENIX: a comprehensive Python-based system for macromolecular structure solution. *Acta Crystallogr. D Biol. Crystallogr.* 66:213-221.
8. Pettersen EF*, et al.* (2004) UCSF Chimera--a visualization system for exploratory research and analysis. *J. Comput. Chem.* 25:1605-1612.
9. Pettersen EF*, et al.* (2021) UCSF ChimeraX: Structure visualization for researchers, educators, and developers. *Protein Sci.* 30:70-82.
10. Shaaban M, Chowdhury S, & Nolen BJ (2020) Cryo-EM reveals the transition of Arp2/3 complex from inactive to nucleation-competent state. *Nat. Struct. Mol. Biol.* 27:1009-1016.
11. Fäßler F, Dimchev G, Hodirnau VV, Wan W, & Schur FKM (2020) Cryo-electron tomography structure of Arp2/3 complex in cells reveals new insights into the branch junction. *Nat. Commun.* 11:6437.
12. Rouiller I*, et al.* (2008) The structural basis of actin filament branching by the Arp2/3 complex. *J. Cell Biol.* 180(5):887-895.
13. Ding B*, et al.* (2022) Structure of Arp2/3 complex at a branched actin filament junction resolved by single-particle cryo-electron microscopy. *Proc Natl Acad Sci U S A* 119:e2202723119.